Polymer Solar Cells with a Low-Temperature-Annealed Sol–Gel-Derived MoO_x Film as a Hole Extraction Layer

Tingbin Yang, Ming Wang, Yan Cao, Fei Huang, Lin Huang, Junbiao Peng, Xiong Gong, Stephen Z. D. Cheng, and Yong Cao*

Great attention has been paid to bulk heterojunction (BHJ) polymer solar cells (PSCs) based on conjugated polymers (electron donor, D) blended with fullerene derivatives (electron acceptors, A) owing to their potential applications as renewable energy sources, and the advantages of easy processing and the possibility of fabricating inexpensive, lightweight flexible devices.[1–5] Power conversion efficiencies (PCEs) of BHJ PSCs over 8% under AM1.5G (standard spectrum of sunlight at the Earth's surface) with an illuminating intensity of 100 mW cm^{-2} have been reported recently.[6–8] However, the major challenge for BHJ PSCs is to demonstrate cells with long-term stability in air.[9–12]

BHJ PSCs are typically fabricated with a transparent conductive anode (e.g. indium tin oxide, ITO), a low-work-function metal cathode (e.g. Al, Ba/Al, and Ca/Ag or Ca/Al), and an active layer (D:A) sandwiched between the anode and the cathode. The BHJ layer dramatically affects the stability of BHJ PSCs. The cathode is inherently flawed, giving low long-term stability. Currently, poly(3,4-ethylenedioxythiophene):poly(styrene sulfonate) (PEDOT:PSS) is often used to smooth the surface of the ITO anode.[13,14] However, it has been demonstrated that the long-term stability problem is caused by the hygroscopic and acidic nature of PEDOT:PSS. PEDOT:PSS etches the ITO, in particular, under ambient conditions and accelerates the diffusion of indium into the photoactive layer, which then induces a fast degradation of the active layer.[15–17]

Two types of approaches have been developed to circumvent these problems. One is to develop BHJ PSCs with an inverted device structure.[18,19] The other is to introduce a stable buffer layer. Recently, metal oxides, such as molybdenum oxide (MoO_3) and vanadium pentoxide (V_2O_5), have been thermally deposited onto the ITO anode to replace the PEDOT:PSS layer. The elimination of the PEDOT:PSS layer improves the device stability.[20] However, a first design for a buffer layer processed from solution is still lacking; solution processing satisfies the requirement of a low-cost manufacturing process.

Among the p-type metal oxides used in BHJ PSCs, MoO_3 is a promising candidate owing to its relatively good hole mobility, environmental stability, and transparency in the range of visible light. Various fabrication methods have been employed to grow thin films of MoO_3.[21–23] The sol–gel method has been extensively investigated as a solution-processed thin film deposition method.[24,25] However, little research has been reported on the use of sol–gel-derived MoO_x thin films in BHJ PSCs. We report a new method of obtaining uniform low-temperature-annealed sol–gel-derived (S-MoO_x) thin films and and demonstrate that they can function as an efficient hole extraction layer in BHJ PSCs.

Low-temperature-annealed sol–gel-derived MoO_x (S-MoO_x) thin films were prepared using molybdenum in H_2O_2 as a precursor solution. The precursor solution was cast onto ITO glass and subsequently treated at 250 °C for 30 min. During the period of thermal treatment, the precursor was converted to the dense S-MoO_x film by hydrolysis. The synthesis is described in detail in the Experimental Section.

The UV–vis absorption spectra of S-MoO_x thin film and thermally deposited MoO_3 (T-MoO_3) thin film are shown in **Figure 1**. The absorption spectrum of S-MoO_x is similar to that of T-MoO_3. A broad absorption ranging from 700 nm to 1000 nm is observed for both T-MoO_3 and S-MoO_x thin films.

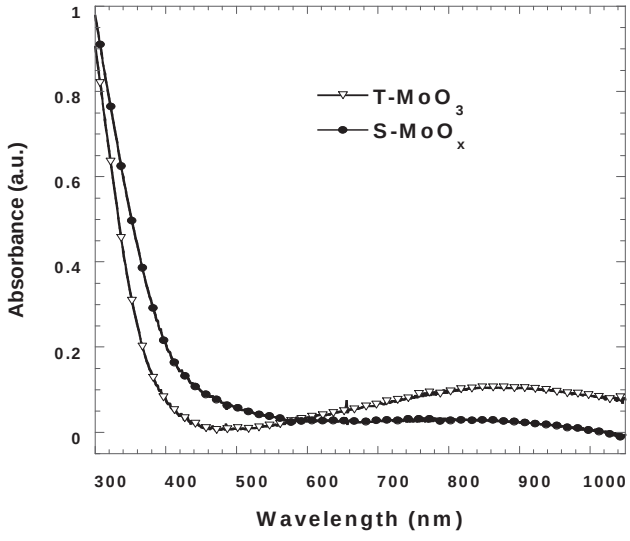

Figure 1. Absorption spectra of the S-MoO_x and T-MoO_3 thin films.

T. B. Yang, Y. Cao, Prof. X. Gong, Prof. S. Z. D. Cheng
College of Polymer Science and Polymer Engineering
The University of Akron
Akron, OH 44325, USA
E-mail: xgong@uakron.edu
T. B. Yang, M. Wang, Prof. F. Huang, Prof. J. B. Peng, Prof. X. Gong, Prof. Y. Cao
State Key Laboratory of Luminescence Physics and Chemistry
South China University of Technology
Guangzhou 510640, P.R. China
Dr. L. Huang
Bruker Nano Surfaces Division
112 Robin Hill Road, Santa Barbara, CA 93117, USA

DOI: 10.1002/aenm.201100598

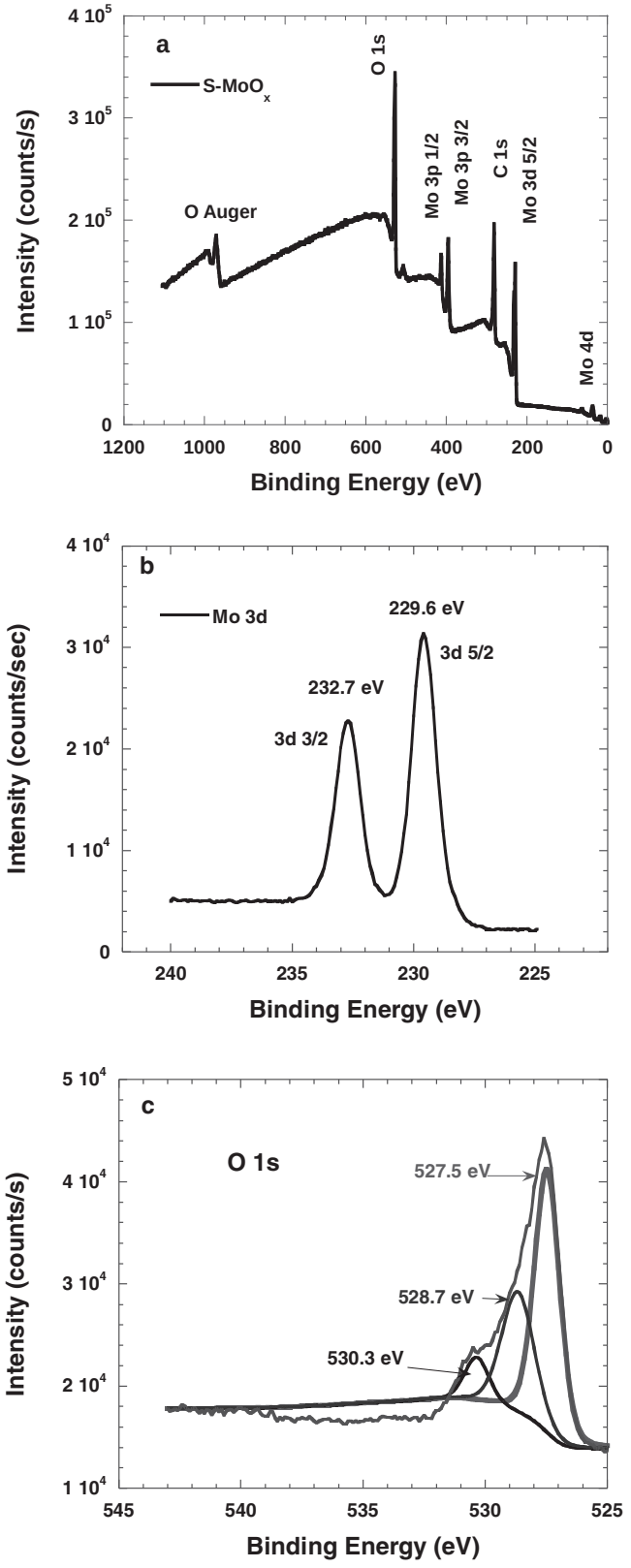

Figure 2. a) The XPS result of a S-MoO$_x$ thin film on top of an ITO substrate. Core levels of b) Mo 3d and c) O 1s.

This broad weak absorption was attributed to the free electrons being trapped in oxygen vacancies in both T-MoO$_3$ and S-MoO$_x$ thin films by UV irradiation.[26] The optical bandgap of S-MoO$_x$ obtained from the UV–vis spectrum is ca. 3.0 eV. The S-MoO$_x$ film is transparent in the visible region except for a weak broad absorption centered at 850 nm, which indicates that the S-MoO$_x$ film can function as a buffer layer on the ITO glass, in that visible light is able to pass through the ITO/S-MoO$_x$ layer into the polymer active layer.

X-ray photoelectron spectroscopy (XPS) measurements were carried out to characterize the major component of S-MoO$_x$. **Figure 2** shows the core level XPS spectra of Mo 3d and O 1s for S-MoO$_x$ film annealed at 250 °C. XPS spectra are referenced to the residual hydrocarbon contamination at 284.6 ± 0.1 eV. The whole spectrum of S-MoO$_x$ shows five individual sharp peaks. Figure 2a displays the C 1s peak located at 281.7 eV, which is about 2.9 eV less than the referenced value, indicating that the other peak positions need to be calibrated by adding this offset. The detailed peak offsets are described in **Table 1**. The binding energies for Mo ($3d_{5/2}$) and Mo ($3d_{3/2}$) are 232.5 eV and 235.6 eV, respectively. The binding energy of 232.5 eV corresponds to the oxide of Mo(VI).

The tuning position of O 1s is at 530.5 eV. However, several O 1s peaks could be fitted from the core level of O 1s spectra, which indicates that more than one oxygen species is present in the S-MoO$_x$ film. Moreover, the peak located at 398.3 eV in the core level of Mo $3p_{3/2}$ corresponds to the state of Mo(VI). All these results demonstrate that a major part of S-MoO$_x$ is MoO$_3$.

The transmission electron microscopy (TEM) bright field (BF) image of S-MoO$_x$ displayed in **Figure 3**a shows that the S-MoO$_x$ thin film is quite uniform. Many nanometer-scale fibrils with a diameter of ca. 20 nm are also observed. No visible pinholes are observed in this TEM BF image. This implies that the S-MoO$_x$ thin film is quite dense, which could prevent leakage current occurring owing to incomplete coverage of the ITO substrate. The atomic force microscopy (AFM) height image is displayed in Figure 3b, with a root mean squared roughness (RRMS) of 0.475 nm at a scale of 2.0 μm × 2.0 μm. This smooth surface implies that the polymer photoactive layer can be easily deposited on top of the S-MoO$_x$ film. In addition, no typical sharp peak of ITO is observed from S-MoO$_x$/ITO, indicating that the rough surface of the ITO substrate has been modified. All these results demonstrate that S-MoO$_x$ thin films have good surface morphologies as a buffer layer in BHJ PSCs.

In order to verify the electronic conductivities of S-MoO$_x$, an AFM tip coated with 20 nm Ir/Pt on both the front and back sides was contacted with the surface of a ca. 30 nm S-MoO$_x$

Table 1. XPS binding energy of the molybdenum compound.

Item	C 1s	O 1s	Mo $3d_{5/2}$	Mo $3d_{3/2}$	Mo $3p_{3/2}$
Expt. Data[a)]	281.7	527.6	229.6	232.7	395.4
Calibrated[b)]	284.6	530.5	232.5	235.6	398.3

[a)]Data obtained directly from experimental measurement; [b)]Data obtained after adjusting the experimental C 1s peak (281.7 eV) to a standard value (284.6 ± 0.1 eV).

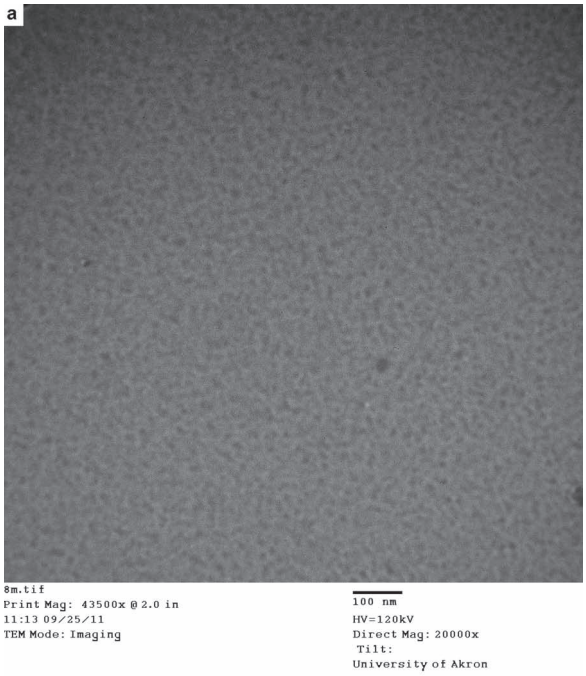

Figure 3. a) A TEM bright field image of the S-MoO_x thin film. b) A tapping-mode AFM image of the S-MoO_x thin film, with a RRMS of 0.457 nm.

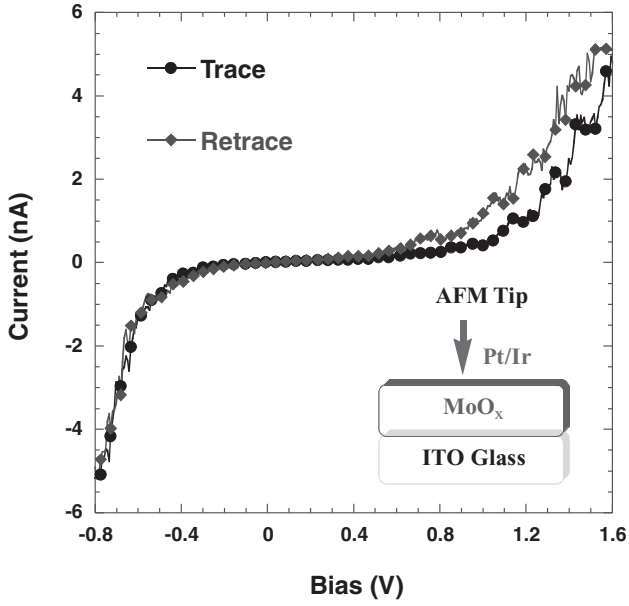

Figure 4. The *I–V* curves of the S-MoO_x/ITO film using an AFM tip coated with Pt/Ir on both the front and back sides. Trace condition: ITO as the anode and Pt/Ir as the cathode. Retrace condition: ITO as the cathode and Pt/Ir as the anode

thin film that was deposited on ITO glass. The peak force tapping tunneling AFM (PFTUNA) module was used to measure the contact currents with bias voltage applied to the ITO/S-MoO_x/Ir/Pt. The *I–V* curves of ITO/S-MoO_x/Ir/Pt for both trace (ITO as the anode and Pt/Ir as the cathode) and retrace conditions (ITO as the cathode and Pt/Ir as the anode) are shown in **Figure 4**. Because the work functions of ITO and Ir are –4.70 eV and –5.27 eV, respectively, asymmetrical *I–V* curves are expected from ITO/S-MoO_x/Ir/Pt under both trace and retrace conditions. The experimental observations are in very good agreement with theoretical analysis.[27] The same asymmetrical *I–V* curves observed under both conditions and the large contact currents observed from very small area AFM tips indicate that S-MoO_x is a semiconductor and possesses good electronic conductivities.

To evaluate the expected high performance of PSCs, BHJ PSCs were fabricated with PBDT-DTNT:$PC_{71}BM$ using S-MoO_x as a hole extraction layer. The molecular structures of PBDT-DTNT[28] and [6,6]-phenyl C_{71}-butyric acid methyl ester ($PC_{71}BM$), the BHJ PSCs' structure, and the energy levels of the component materials are shown in **Figure 5**. Because the major component of low-temperature-annealed sol–gel-derived S-MoO_x is MoO_3 (see Figure 2), the lowest unoccupied molecular orbital (LUMO) energy and the highest occupied molecular orbital (HOMO) energy levels of bulk MoO_3[29,30] are used to describe the energy levels of S-MoO_x. As shown in Figure 5c, because the HOMO energy of S-MoO_x is close to that of PBDT-DTNT, holes are expected to be efficiently transported to the ITO anode without significant loss in energy. Moreover, because the LUMO energy of S-MoO_x is higher than that of PBDT-DTNT, the S-MoO_x film can function as an electron blocking layer. Therefore, the S-MoO_x film can be used as the hole extraction layer in BHJ PSCs.

The current density–voltage characteristics (*J–V*) of the BHJ PSCs with either S-MoO_x or PEDOT:PSS as a buffer layer are shown in **Figure 6**. Under AM1.5G illumination with light intensity of 100 mW cm^{-2}, an open-circuit voltage V_{oc} of 0.75 V, a short-circuit current density J_{sc} of 16.44 mA cm^{-2}, a fill factor FF of 47.5%, and a corresponding PCE of 5.86% are obtained from the PSCs with S-MoO_x as the buffer layer. The high V_{oc} observed suggests a good band alignment between the polymer active layer and the electrodes. The small difference between

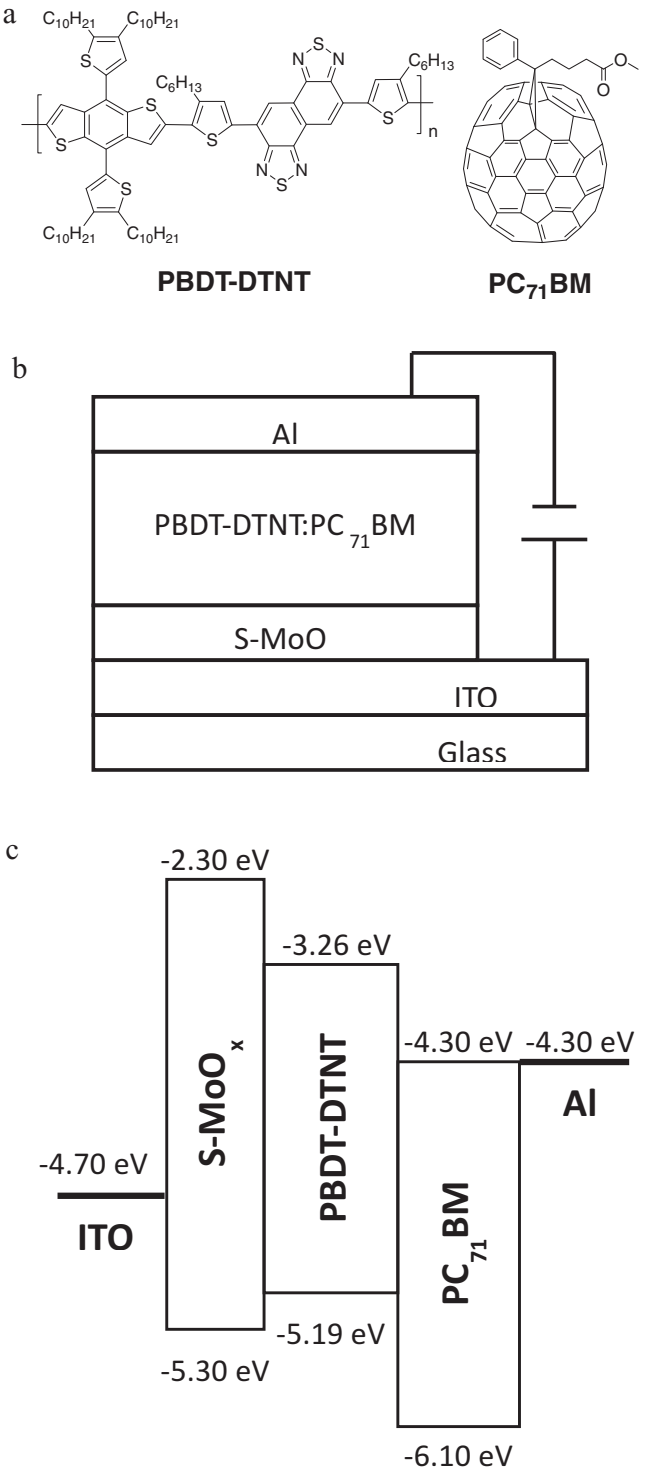

Figure 5. a) The molecular structures of PBDT-DTNT and $PC_{71}BM$. b) The device structure of polymer solar cells. c) Energy-level diagram with the LUMO and HOMO of each component.

the calculated V_{oc} (0.89 V)[31] and the observed V_{oc} (0.75 V) implies that only 0.14 V is lost even when the electrode contact resistance is involved. The high J_{sc} observed indicates that the charge transport across the S-MoO_x layer is unhindered. In

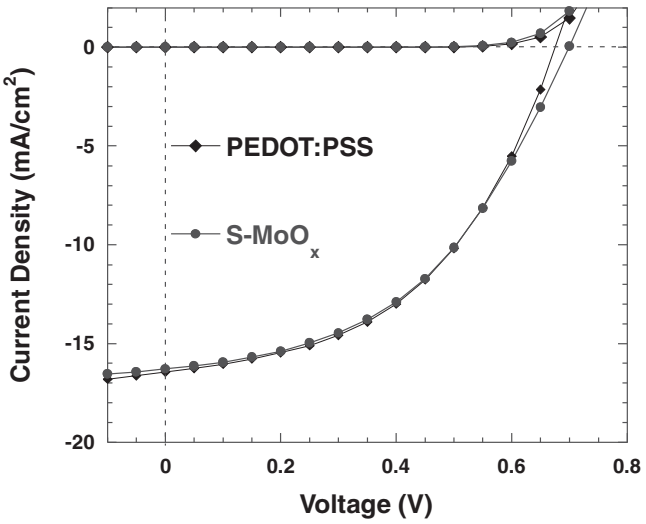

Figure 6. *J–V* characteristics of PSCs with S-MoO_x and PEDOT:PSS layer as the buffer layer.

order to confirm this hypothesis, BHJ PSCs with PEDOT:PSS as a buffer layer were also fabricated to be investigated. Under the same illumination condition, a V_{oc} of 0.73 V, a J_{sc} of 16.64 mA cm^{-2}, a FF of 48.5%, and a corresponding PCE of 5.89% are observed. These device performance parameters are comparable with those observed from PSCs with S-MoO_x as the buffer layer. Therefore, our findings demonstrate that a low-temperature-annealed sol–gel-derived MoO_x thin film can be used as a hole extraction layer in BHJ PSCs in the quest for high performance.

In conclusion, a low-temperature-annealed sol–gel-derived MoO_x (S-MoO_x) thin film as a hole extraction layer in BHJ PSCs was successfully made and demonstrated. The characterization of S-MoO_x thin films by absorption spectra, XPS, TEM, AFM, and PFTUNA indicated that S-MoO_x films can be used as a buffer layer for BHJ PSCs. A PCE of 5.86% observed from BHJ PSCs with a device structure of ITO/S-MoO_x/PBDT-DTNT:$PC_{71}BM$/Al is comparable with a PCE of 5.89% obtained from BHJ PSCs with a device structure of ITO/PEDOT:PSS/PBDT-DTNT:$PC_{71}BM$/Al. These results demonstrate that a low-temperature-annealed sol–gel-derived MoO_x thin film can be used as a hole extraction layer in BHJ PSCs.

Experimental Section

Materials: The synthesis of PBDT-DTNT was reported elsewhere.[28] $PC_{71}BM$ and molybdenum powder were purchased from Sigma-Aldrich Inc.

S-MoO_x Preparation: Molybdenum powder (10 g) was first prepared in a clean beaker, then H_2O_2 (100 mL, concentration 30%) was slowly added. A cool water bath was needed to avoid the accumulation of a great deal of heat. The above solution was centrifuged at 3000 rpm to remove the unreacted reactant. The solution was subsequently dried by distillation. The obtained product was then dissolved in methanol (10 mg mL^{-1}) for preparation of the S-MoO_x thin film.

UV–vis Absorption Spectra: The UV–vis absorption spectra of low-temperature-annealed sol–gel-derived MoO_x thin films and thermally deposited MoO_3 thin films were measured with a HP 8453 UV–vis spectrophotometer.

XPS: XPS analysis was carried out on an XPS/ESCA (electron spectroscopy for chemical analysis) instrument (Axis Ultra DLD from Kratos Inc.) utilizing a monochromatized Al Kα X-ray source. Spectra were referenced to the residual hydrocarbon contamination at 284.6 ± 0.1 eV. A thin film (ca. 30 nm) was deposited on the ITO substrate for XPS analysis.

Morphologies: TEM experiments were carried out with a JEOL transmission electron microscope using an accelerating voltage of 120 kV. Tapping-mode AFM images were obtained using a NanoScope NS3A system (Digital Instruments) to observe the surface morphology of S-MoO_x.

Electronic Conductivities: The electronic conductivities of S-MoO_x thin films were measured on a Bruker Dimension Icon system with a PeakForce Tapping and Tunneling AFM (PFTUNA) module. The probe was the PFTUNA probe with a spring constant of ca. 0.5 N m^{-1} and a 20 nm Pt/Ir coating on both the front and back sides. The spring constant was measured using a thermal tune method. The *I–V* curves were collected using constant deflection force as the feedback control. The contact currents were measured with a bias voltage applied to the sample. The number of pixels (512), the ramp rate of 0.4 Hz, and the force setpoint of ca. 60 nN were set for both the trace (scan from *–V* to *+V*) and retrace (scan from *+V* to *–V*).

Device Fabrication: BHJ PSCs were fabricated by the following procedure. The ITO substrate was cleaned by ultrasonication in acetone, detergent, deionized water, and isopropyl alcohol sequentially. The S-MoO_x thin film was obtained by spin-casting the MoO_x precursor on top of the ITO substrate. The substrate was then annealed at 250 °C for 30 min and formed S-MoO_x thin films with a thickness of about 30 nm. The PEDOT:PSS layer was spin-coated with a thickness of about 40 nm from aqueous solution (after passing a 0.45 μm filter). The PEDOT:PSS-covered substrate was dried for 10 min at 140 °C in air. Both of the substrates were transfered into a glove-box to spin-cast the photoactive layer. The 1,2-dichlorobenzene solution comprising PBDT-DTNT (15 mg mL^{-1}) and $PC_{71}BM$ (15 mg mL^{-1}) was then spin-cast on top of the S-MoO_x and PEDOT:PSS layers. After that, the devices were thermally annealed at 110 °C for 10 min. Finally, the devices were pumped down to a ca. 3×10^{-6} mbar pressure, and a ca. 100 nm Al film was deposited on top of the photoactive layer.

Acknowledgements

XG acknowledges the University of Akron, 3M for financial support and the Joint Research Fund for Overseas Chinese Scholars, the National Science Foundation of China (No. 50828301). TBY thanks Yongxiang Zhu at SCUT for many discussions and the China Scholarship Council for Joint PhD program. SCUT thanks NSFC (51010003, 50990065, 51073058, and 20904011) and MOST (2009CB623601) for financial support.

Received: October 7, 2011
Revised: December 22, 2011
Published online: March 2, 2012

[1] K. M. Coakley, M. D. McGehee, *Chem. Mater.* **2004**, *270*, 1789.
[2] P. W. M. Blom, V. D. Mihailetchi, L. J. A. Koster, D. E. Markov, *Adv. Mater.* **2007**, *19*, 1551.
[3] S. Gunes, H. Neugebauer, N. S. Sariciftci, *Chem. Rev.* **2007**, *107*, 1324.
[4] G. Dennler, M. C. Scharber, C. J. Brabec, *Adv. Mater.* **2009**, *21*, 1.
[5] T. D. Nielsen, C. Cruickshank, S. Foged, J. Thorsen, F. C. Krebs, *Sol. Energy Mater. Sol. Cells* **2010**, *94*, 1553.
[6] http://www.solarmer.com. Accessed January 2012.
[7] http://www.konarka.com. Accessed January 2012.
[8] Z. He, C. Zhong, X. Huang, W. Y. Wong, H. Wu, L. Chen, S. Su, Y. Cao, *Adv. Mater.* **2011**, *23*, 4636.
[9] C. J. Brabec, S. Gowrisanker, J. J. M. Halls, D. Laird, S. Jia, S. P. Williams, *Adv. Mater.* **2010**, *22*, 3839.
[10] F. C. Krebs, H. Spanggaard, *Chem. Mater.* **2005**, *17*, 5235.
[11] J. A. Hauch, P. Schilinsky, S. A. Choulis, R. Childers, M. Biele, C. J. Brabec, *Sol. Energy Mater. Sol. Cells* **2008**, *92*, 727.
[12] B. Zimmermann, U. Würfel, M. Niggemann, *Sol. Energy Mater. Sol. Cells.* **2009**, *93*, 491.
[13] G. Heywang, F. Jonas, *Adv. Mater.* **1992**, *4*, 116.
[14] F. Zhang, M. Johansson, M. R. Andersson, J. C. Hummelen, O. Inganäs, *Adv. Mater.* **2002**, *14*, 662.
[15] M. P. de Jong, L. J. van IJzendoorn, M. J. A. de Voigt, *Appl. Phys. Lett.* **2000**, *77*, 2255.
[16] G. Greczynski, T. Kugler, M. Keil, W. Osikowicz, M. Hahlman, W. R. Salaneck, *J. Electron Spectrosc. Relat. Phenom.* **2001**, *121*, 1.
[17] M. Jorgensen, K. Norrman, F. C. Krebs, *Sol. Energy Mater. Sol. Cells* **2008**, *92*, 686.
[18] S. K. Hau, H. L. Yip, N. S. Baek, J. Zou, K. O'Malley, A. K. Y. Jen, *Appl. Phys. Lett.* **2008**, *92*, 253301.
[19] L. M. Chen, Z. Hong, G. Li, Y. Yang, *Adv. Mater.* **2009**, *21*, 1434.
[20] Y. Sun, C. J. Takacs, S. R. Cowan, J. H. Seo, X. Gong, A. Roy, A. J. Heeger, *Adv. Mater.* **2011**, *23*, 2226.
[21] N. Miyata, S. Akiyoshi, *J. Appl. Phys.* **1985**, *58*, 1651.
[22] C. E. Tracy, D. K. Benson, *J. Vac. Sci. Technol. A* **1986**, *4*, 2377.
[23] M. Ferroni, V. Guidi, G. Martinelli, P. Nelli, M. Sacerdoti, *Thin Solid Films* **1997**, *307*, 148.
[24] C. J. Brinker, G. W. Scherer, *Sol–Gel Science: The Physics and Chemistry of Sol–Gel Processing*, Academic, San Diego CA **1990**.
[25] L. L. Hench, J. K. West, *Chem. Rev.* **1990**, *90*, 337.
[26] S. K. Deb, J. A. Chopoorian, *J. Appl. Phys.* **1966**, *37*, 4818.
[27] S. M. Sze, K. K. Ng, *Physics of Semiconductor Devices*, 3rd ed., Wiley, Hoboken, NJ **2007**.
[28] M. Wang, X. Hu, P. Liu, W. Li, X. Gong, F. Huang, Y. Cao, *J. Am. Chem. Soc.* **2011**, *133*, 9638.
[29] V. Shrotriya, G. Li, Y. Yao, C. W. Chu, Y. Yang, *Appl. Phys. Lett.* **2006**, *88*, 073508.
[30] Irfan, H. Ding, Y. Gao, D. Y. Kim, J. Subbiah, F. So, *Appl. Phys. Lett.* **2010**, *96*, 073304.
[31] M. C. Scharber, D. Mühlbacher, M. Koppe, P. Denk, C. Waldauf, A. J. Heeger, C. J. Brabec, *Adv. Mater.* **2006**, *18*, 789.